

Article

# Hydrothermal Co-Crystallization of Novel Copper Tungstate-Strontium Titanate Crystal Composite for Enhanced Photocatalytic Activity and Increased Electron–Hole Recombination Time

Áron Ágoston  and László Janovák \* 

Department of Physical Chemistry and Materials Sciences, University of Szeged, Rerrich B. Sqr.1, H-6720 Szeged, Hungary

\* Correspondence: janovakl@chem.u-szeged.hu; Tel.: +36-62-544-210

**Abstract:** The development of catalysts continues to have a significant influence on science today since we can utilize them to efficiently destroy some contaminants. A study in this field is justified because there is a dearth of comprehensive literature on the creation of SrTiO<sub>3</sub>-based photocatalysts. Related to this topic, here we report the facile preparation of a structure-modified SrTiO<sub>3</sub> photocatalyst, by incorporating CuWO<sub>4</sub>. Within the case of the CuWO<sub>4</sub>-modified samples (0.5–3 wt% nominal CuWO<sub>4</sub> content), the photo-oxidation of phenol, as a contaminant, was more than two times higher than the initial SrTiO<sub>3</sub>. However, the photocatalytic activity does not change linearly with increasing CuWO<sub>4</sub> content, and the CWS2.5 (2.5 wt% nominal CuWO<sub>4</sub> content and 4.25 wt% measured content) has the highest photo-activity under the applied conditions. The reason for the better activity was the increased recombination time of charge separation on the catalyst surface. Slower recombination can result in more water being oxidized to hydroxyl radicals, leading to the faster decomposition of the phenol.

**Keywords:** strontium-titanate; copper tungstate; hydrothermal co-crystallization; copper tungstate content optimization; hydroxyl radical; recombination time



**Citation:** Ágoston, Á.; Janovák, L. Hydrothermal Co-Crystallization of Novel Copper Tungstate-Strontium Titanate Crystal Composite for Enhanced Photocatalytic Activity and Increased Electron–Hole Recombination Time. *Catalysts* **2023**, *13*, 287. <https://doi.org/10.3390/catal13020287>

Academic Editor: Roberto Fiorenza

Received: 30 December 2022

Revised: 20 January 2023

Accepted: 24 January 2023

Published: 27 January 2023



**Copyright:** © 2023 by the authors. Licensee MDPI, Basel, Switzerland. This article is an open access article distributed under the terms and conditions of the Creative Commons Attribution (CC BY) license (<https://creativecommons.org/licenses/by/4.0/>).

## 1. Introduction

The study of photocatalysts is still a popular field of research today, because their good properties can be used in many fields, e.g., antimicrobial treatment, air cleaning and water purification [1–5]. Most photocatalysts are metal nanoparticles or semiconducting metal oxides, such as strontium titanate (SrTiO<sub>3</sub>), which is widely studied nowadays. SrTiO<sub>3</sub> has many useful advantages such as low cost, inertness, stability and relatively high photocatalytic activity in the UV region. It is justified to deal with this material because the photocatalytic activity can be increased after various modifications. We have several options for increasing the photocatalytic activity, such as reducing the band gap (excitation with lower energy photons), increasing the number of charge separations created per unit time or increasing the recombination time (more reactive radicals are produced) [6,7]. The long-term goal is to learn more about the nature of modifications where we do not achieve higher photocatalytic activity by reducing the band gap but by increasing the recombination time so that we can later enhance this in the best way.

Heterogeneous photocatalysis is an advanced oxidation process (other AOPs: homogeneous photocatalysis, photolysis, Gamma-radiolysis) [8]. In the case of heterogeneous photocatalysis, the photocatalyst can be excited with photons, and this induces a hole–electron pair through the change in the energy state of the electron (the electron energy moves from the valence band to the conduction band) [9]. The residual hole is the oxidation side, where the hole oxidizes the adsorbed molecules (usually water molecules), and the

result is the generation of reactive radicals. The excited electron is on the reduction side, where some molecules are able to accept electrons, which results in a negative oxidation potential (so it will have a reductive characteristic). Through the processes described, reactive oxygen species could be generated, e.g., hydroxyl radical,  $\text{H}_2\text{O}_2$ , peroxide radical, hydroxyl anion and superoxide anion [10]. One option is to reduce the band gap (excitation with visible light), while another option is to increase the recombination time (more reactive radicals are produced).

We have three useful ways for modification: decoration, which is when the surface of the photocatalyst is modified (e.g., metal deposition), doping, which is when the crystalline structure is modified, and morphological modifications [11–13]. During the surface modification, metals or metal oxides are usually deposited on the surface, and some transition metals or transition metal oxides (Ag, Au, CuO) have a plasmonic effect on the surface of the catalyst, which also increases the recombination time [13]. Doping photocatalysts with various elements (e.g., Ag, Ru, C, N, Cu) can reduce the band gap energy, and, therefore, the photocatalyst could be activated with a photon with lower energy, and the dopant can act as an electron trap, which slows down the recombination of the electron–hole pairs, which also favors photocatalytic activity [12]. In the case of morphological modification, generally, the shape and porosity are modified [11]. In the scientific literature, we can find many articles on modified  $\text{SrTiO}_3$ . The comparison of photocatalytic activities measured by others in other labs is difficult, due to the different conditions, e.g., the light source, the concentration of the catalyst, the reactor, the construction of the system, the model pollutants and its concentration are different. For example, Syafiuddin et al. doped the  $\text{SrTiO}_3$  with sulfur and nitrogen (separated); in the former case, the catalyst decomposed ~12% of the phenol and, in the latter case, ~10% under 2 h [14]. Another study investigated the decomposition of Rhodamine B on a graphene oxide/strontium titanate composite and on pure  $\text{SrTiO}_3$ ; the former decomposed 94.5% of the pollutant and the latter 64.5% under the applied conditions [15]. According to another article,  $\text{CuO}_x$ -modified  $\text{SrTiO}_3$  was used to investigate the degradation of phenol, achieving a degradation efficiency of ~19% [7].

In this work, we modified the  $\text{SrTiO}_3$  photocatalyst with different amounts of tungstate ( $\text{CuWO}_4$ ) by a hydrothermal co-crystallization method, and the  $\text{CuWO}_4$  content was optimized. This is novel because  $\text{CuWO}_4$  has not yet been used to modify  $\text{SrTiO}_3$ . Structure and optical characterization methods were applied to prove the success of the photocatalyst preparation and to determine the properties of the prepared photocatalysts. Next, we determined the photocatalytic activity for all the prepared photocatalysts under UV illumination following the degradation of the phenol test molecule and the ability to produce hydroxyl radicals through coumarin degradation. The results show that the  $\text{CuWO}_4$ -modified  $\text{SrTiO}_3$  has higher photocatalytic activity than pure  $\text{SrTiO}_3$ .

## 2. Results and Discussion

### 2.1. Characterization

The crystal phase of the obtained photocatalysts was determined by XRD measurements. Figure 1A shows the diffractogram of the pure  $\text{SrTiO}_3$  (CWS0) and the composite samples with increased  $\text{CuWO}_4$  content (CWSX). The patterns of the diffractograms are the same, and therefore the crystal structure is the same. However, the main reflection shifts slightly to the left (from  $2\theta = 32.48^\circ$  to  $32.36^\circ$ ), like a trend, which suggests that the distance between the corresponding crystal faces has changed (Figure 1C). This is due to the presence of a crystalline foreign material [16], which in our case is probably  $\text{W}^{6+}$  instead of  $\text{Ti}^{4+}$  from  $\text{CuWO}_4$ , because their ionic radius is similar ( $0.61 \text{ \AA}$  for  $\text{Ti}^{4+}$  and  $0.60 \text{ \AA}$  for  $\text{W}^{6+}$ ), and by increasing the proportion of  $\text{CuWO}_4$ , the crystal faces get closer and closer. Furthermore, the SEM pictures taken of some samples show that with the increasing  $\text{CuWO}_4$  content the surface of the catalyst becomes flaky (Figure S1A–C), while the EDX mapping indicates the increasing Cu content (Figure S1E,F). The trend of the shift is broken for the CWS3 sample, which indicates overdoping, so  $\text{CuWO}_4$  is present in a larger amount than can be integrated into the lattice; this also affects the crystallization, and probably amorphous

$\text{CuWO}_4$  remains on the sample. This phenomenon is also clearly visible when the results are presented later. As a check, we crystallized pure copper tungstate (Figure 1B), and its XRD pattern is different from the composite samples; hence, in the absence of  $\text{SrTiO}_3$ , it crystallizes in a different crystal phase.

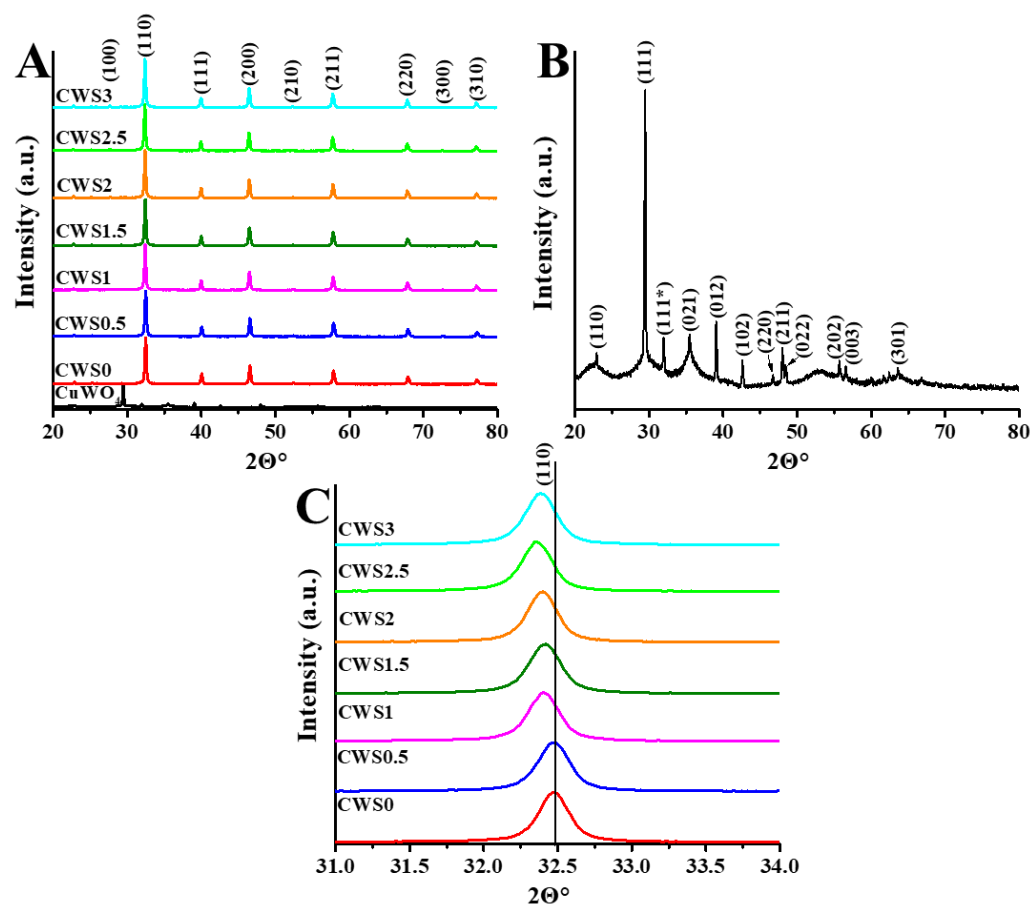


**Figure 1.** XRD patterns of  $\text{SrTiO}_3$  (CWS0) and  $\text{CuWO}_4$ - $\text{SrTiO}_3$  composite samples (CWSX) (A),  $\text{CuWO}_4$  (B) and the main reflection shift (C).

The results indicate that during co-crystallization, they crystallize in the same crystal structure, in the crystal structure of  $\text{SrTiO}_3$ ; that is, the crystallization of  $\text{SrTiO}_3$  affects the crystallization of  $\text{CuWO}_4$ . There could be several reasons for this; for example, the crystallization energy of  $\text{SrTiO}_3$  [17], which is two orders of magnitude larger, affects the crystallization of  $\text{CuWO}_4$ , or more crystal sources are formed from  $\text{SrTiO}_3$  and a composite crystal is formed, which would explain the reflection shift due to the different ion sizes [16]. The CWSX sample peaks belong to the  $\text{SrTiO}_3$  ((100), (110), (111), (200), (210), (211), (220), (300), (310) [18]), and these peaks were assigned with the help of the  $\text{SrTiO}_3$  JCPDS card (35-0734). The  $\text{CuWO}_4$  sample peaks were identified based on the  $\text{CuWO}_4$  JCPDS card (70-1732): (110), (111), (111\*), (021), (012), (102), (220), (211), (022), (202), (003), (301) [19].

Furthermore, the  $\text{CuWO}_4$ -modified samples were turquoise in color (the color intensifies with the  $\text{CuWO}_4$  content), which also indicates the successful modification of the initial white strontium titanate. The light absorption of the CWSX samples was measured by the diffuse reflectance spectroscopy (DRS) method (Figure 2). The band gap energy values were determined by the Kubelka–Munk method [20], and the result was around 3.20 eV for each sample. The band gap slightly changed, but not significantly, and therefore the increased photocatalytic activity (see later) has another reason, not the decreased band gap. Therefore, the incorporation of  $\text{CuWO}_4$  into the structure of  $\text{SrTiO}_3$  did not significantly affect (in the case of the samples produced in this work) the energy dependence of the

excitability. It can also be observed that the spectra of the CWS3 sample with the highest functionalization degree are slightly different from the others, which is certainly due to overdoping, since more  $\text{CuWO}_4$  is present than can be incorporated into the lattice.

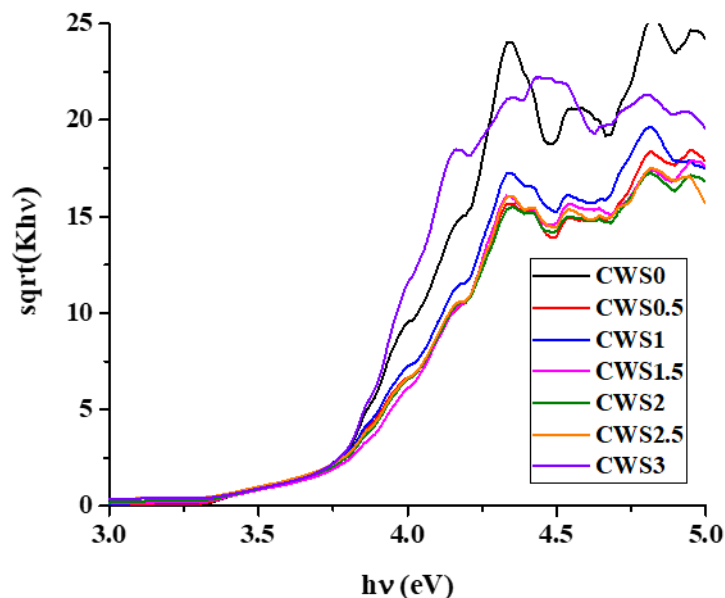


**Figure 2.** Kubelka–Munk representation of  $\text{SrTiO}_3$  (CWS0) and SRTX samples for band gap energy determination.

By measuring the photoluminescence, we can get information about the recombination after excitation [21], and we can compare the samples in the energy consumption received from the photon. On the basis of the measured emission spectra, it can be seen that the presence of  $\text{CuWO}_4$  reduced the degree of recombination, and it can also be seen that the more  $\text{CuWO}_4$ , the more the recombination decreases (up to the level of copper tungstate concentrations used); the normalized results are in Figure 3. This means that the excited electron can return to the valence band in other ways, which is the reason for the increased photocatalytic activity (applied conditions). Due to the closeness of the potentials, the excited electron of strontium titanate (CB of  $\text{SrTiO}_3$  is also 3.4 eV [22]) can be transferred to the valence band of  $\text{CuWO}_4$  (VB of  $\text{CuWO}_4$  is also 2.3 eV [23]), which is possible because the outer electron of  $\text{CuWO}_4$  is also excited at the same time as the excitation of  $\text{SrTiO}_3$ , so a positive hole remains in its valence band. The excited electron of  $\text{CuWO}_4$  is therefore more difficult to recombine, and it is much more likely to be taken up by oxygen, because it has more time for that, after which a hole remains at the end of the “chain” ( $\text{SrTiO}_3$  VB), which produces a hydroxyl radical through the oxidation of water [24]. In the case of pure  $\text{SrTiO}_3$ , the dissolved oxygen (or other molecules from the medium) can only pick up the electron from the  $\text{SrTiO}_3$ , so the electron has two options: it recombines or is picked up by a molecule of the medium. However, the  $\text{CuWO}_4$ - $\text{SrTiO}_3$  composite has a third option when the electron is switching to  $\text{CuWO}_4$  (which can happen, e.g.,  $\text{BiVO}_4$ -based photocatalysts [25]). Because of this, the possibility of recombination is statistically minimally decreased [26], which is clearly visible on the normal photoluminescence spectra (the measured intensity is reduced). Therefore, electron transfer and hydroxyl radical production also take place in the case of  $\text{SrTiO}_3$  (proven later in Section 2.3), but in the presence of  $\text{CuWO}_4$ , there are more possibilities for this in a unit time with minimally suppressed recombination. This is the reason for the increased photocatalytic activity.

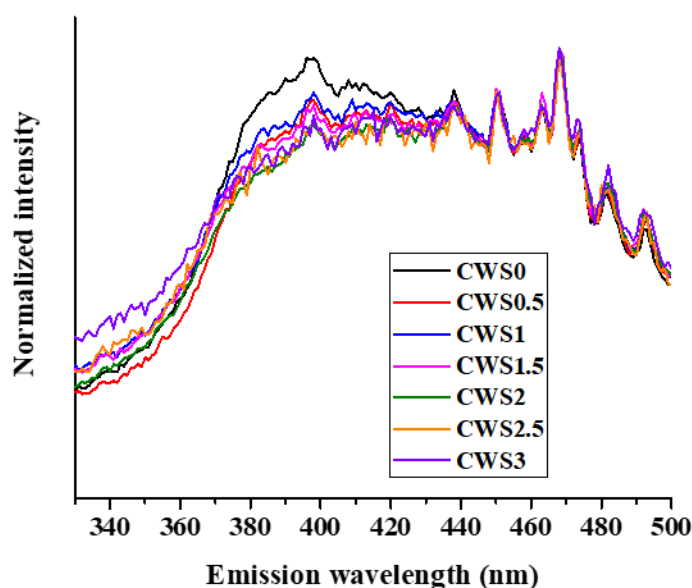


**Figure 3.** The PL spectra of the CWSX samples.

The shape of the emission spectra is very similar for CWS0 and the other CWSX samples, which also shows (in addition to XRD) the relationship between the two substances, so it is not a physical mixture, and they did not crystallize next to each other but crystallized “together” (co-crystallization). Another reason that the shape of the spectra is very similar is that the  $\text{CuWO}_4$  concentration used is very low, and the resulting tungsten concentration is therefore even lower. In the case of doping, the foreign element is usually not integrated in full amount, and in our case, the change is very small.

The specific surface area values are presented in Table 1. The samples have similar surface areas; each sample was measured three times, and the difference is comparable to the value of the standard deviations (Table 1). Thus, the specific surface area of the samples is approximately the same (around  $40 \text{ m}^2/\text{g}$ ), which also proves that it is the same structure and probably co-crystallization, namely  $\text{CuWO}_4$  incorporated into the structure of  $\text{SrTiO}_3$ , and the result is composite crystallites. Due to the similarity of the values, the crystallite size probably did not change significantly with the modified structure.

**Table 1.** Nominal and measured  $\text{CuWO}_4$  concentrations and specific surface area of the samples.

Catalyst Name	Nominal Cu Content (wt%)	Measured $\text{CuWO}_4$ Content (wt%) *	Specific Surface Area ( $\text{m}^2/\text{g}$ )
CWS0	0	0	$40.30 \pm 1.60$
CWS0.5	0.50	0.21	$38.38 \pm 0.40$
CWS1	1.00	1.34	$41.04 \pm 0.35$
CWS1.5	1.50	2.16	$39.30 \pm 0.55$
CWS2	2.00	2.86	$40.81 \pm 1.95$
CWS2.5	2.50	4.28	$40.92 \pm 5.43$
CWS3	3.00	5.22	$40.13 \pm 1.18$

\* determined by EDX measurements.

Figure 4 shows the zeta-potential values of the CWSX samples; the standard deviation was calculated from five measurements. Compared to the initial  $\text{SrTiO}_3$  (CWS0) ( $\zeta = -30.3 \pm 1.6$ ), the zeta potential of functionalized samples slightly decreased ( $\sim -33$ – $38 \text{ mV}$ ); however, CWS3 with the highest  $\text{CuWO}_4$  content had a significantly lower value ( $-38.1 \text{ mV}$ ) because of the above-mentioned overdoping. Further increasing the ratio would probably further decrease the zeta potential, which would favor the adsorption of a positively charged pollutant, but in this work, we did not examine this observation, because we used phenol as a model pollutant and we examined how the photocatalytic activity changed

for phenol; in any case, this information can also be useful for the literature and other researchers. The lower surface charge increases the stability of the suspension when the sample is used as a suspension. The pH was around 6.50 for each sample.

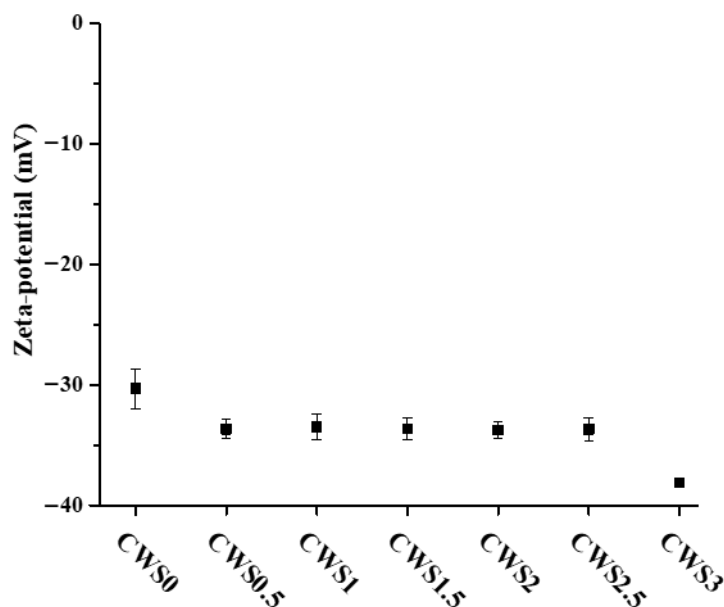


**Figure 4.** The zeta-potential values of 0.001 wt% aqueous dispersion of the initial SrTiO<sub>3</sub> (CWS0) and CWSX samples (pH = ~6.50).

The measured amount of CuWO<sub>4</sub> presented in a weight ratio is proven by EDX measurements; for demonstration, the CWS3 sample EDX spectrum is in Figure 5. The measured values do not always correspond to the nominal (theoretical amount of CuWO<sub>4</sub>) values but follow a well-managed trend; the results are in Table 1. It can also be read from the spectra that it does not contain significant amounts of other elements. The ratio of CuWO<sub>4</sub> in the measured samples is probably higher than the theoretical value, because during the synthesis, the SrTiO<sub>3</sub> precursors remained on the wall of the vessel during the pouring from one vessel to another and also during pouring from the vessel into the autoclave.

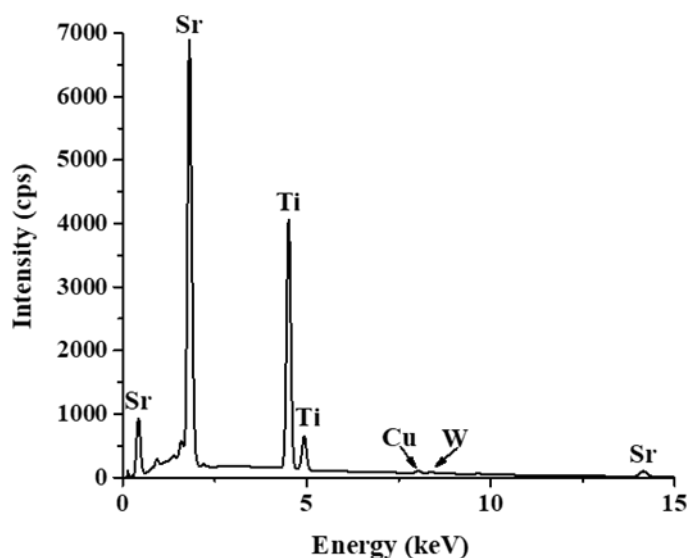


**Figure 5.** Representative EDX spectrum of the CWS3 sample.

## 2.2. Photocatalytic Activity Measurements

The conditions during the photocatalytic experiments were the same for all samples. For reference, the CWS0 sample was used, in which the concentration of  $\text{CuWO}_4$  was 0 wt%. The results are summarized in Figure 6, and almost all of the synthesized photocatalyst samples had higher photocatalytic activity than the reference CWS0 (pure  $\text{SrTiO}_3$ ). CWS2.5 exhibited the highest photocatalytic activity (in Figure 6A are the decay curves, and in Figure 6B is the degraded amount of phenol). The reference CWS0 degraded only a small amount of phenol, and the conversion rate was  $\sim 10\%$  ( $1.063 \text{ mg}_{\text{phenol}}/\text{g}_{\text{cat}}$ ). In the case of CWSX samples, significantly better results were obtained, with conversion rates of  $\sim 10\text{--}24\%$ . The highest value, which belongs to the CWS2.5, was  $24\%$  ( $2.340 \text{ mg}_{\text{phenol}}/\text{g}_{\text{cat}}$ ). Because neither the band gap nor the surface charge exhibits an “extreme” value in this sample, the superior photocatalytic activity has to be explained in another way. Because hydroxyl radicals are involved in the conversion of phenol [27], their quantity in our system can be crucial. According to the XRD results, the trend of the main reflection shift indicates doping (see Section 2.1), which means a small structural change. This trend continues linearly to the CWS2.5 sample and then breaks in the last sample (CWS3), due to overdoping, which has a negative effect on the photocatalytic activity. Due to the mentioned reasons, fewer pollutants can be oxidized on the hole side after the charge separation (direct effect), and fewer hydroxyl radicals can be formed by the oxidation of water. The next section discusses this occurrence through the hydroxyl radical production. The photocatalytic activity does not follow the usual trend, the effect of the modification is not immediately visible in the first member of the modified sample series. The increase in photocatalytic activity starts from the third member (CWS1.5, 1.5 wt.% nominal and 2.16 wt.% measured  $\text{CuWO}_4$  content) of the modified sample series and then “breaks off” at the last member. This can be explained that at the beginning when the doping is so small, it cannot yet have a significant effect on the processes after charge separation; however, the later samples already have this “threshold concentration”. For the last sample, the explanation may be the phenomenon of overdoping described earlier. The results show that, under certain conditions, the CWS2.5 sample has the optimal  $\text{CuWO}_4$  content (measured to be 4.28% by weight) to achieve maximum phenol degradation activity.

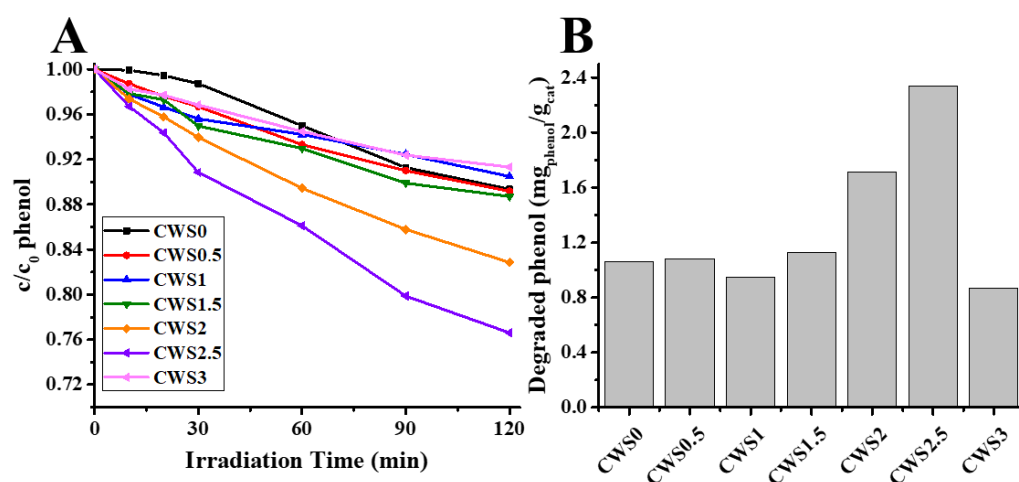


**Figure 6.** Run of decay curves, photocatalytic activity of the CWSX photocatalysts and reference  $\text{SrTiO}_3$  (CWS0) (A) and the exact amount of phenol that has been destroyed ( $\text{mg}_{\text{phenol}}/\text{g}_{\text{cat}}$ ) (B).

## 2.3. Detection of Hydroxyl Radical

Without a catalyst, the 7-hydroxyoumarin molecule was not detectable, and only the hydroxyl radicals created during the photocatalytic reaction can provide 7-hydroxyoumarin [28]. The measurements were performed on all samples, and in Figure 7, the 7-hydroxyoumarin formation kinetic can be seen. The formation kinetics of 7-hydroxyoumarin is the highest

in the case of CWS2.5; the corresponding rate constant ( $k_{7\text{-hydroxycoumarin}}$ ) was  $1.52 \times 10^{-5} \mu\text{mol}\cdot\text{L}^{-1}\cdot\text{s}^{-1}$  which is an order of magnitude greater than the reference (CWS0) sample ( $5.29 \times 10^{-6} \mu\text{mol}\cdot\text{L}^{-1}\cdot\text{s}^{-1}$ ). The mentioned values were calculated based on the measurements presented in Figure 7. The trend closely follows the trend obtained for photocatalytic efficiency, for the same reason as described in the previous section (Section 2.2).

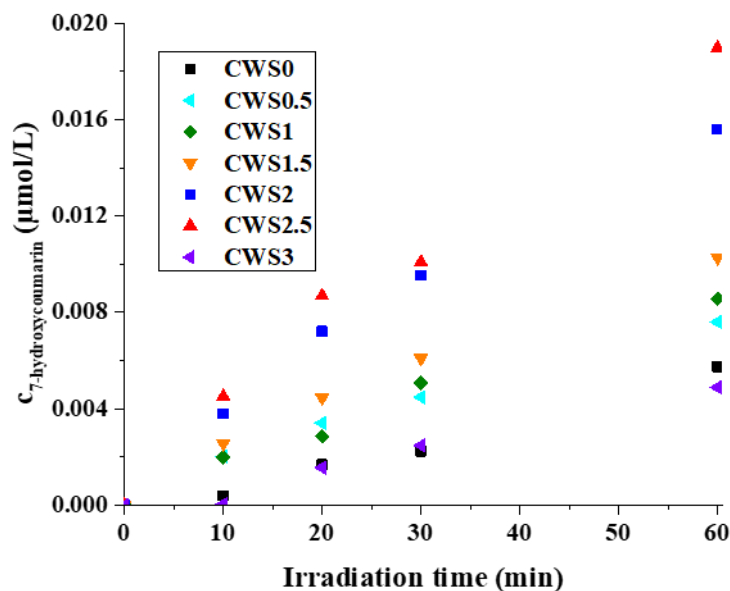


Figure 7. Production kinetics of 7-hydroxycoumarin from coumarin in the case of CWSX samples.

### 3. Materials and Methods

#### 3.1. Catalyst Preparation

Analytical grade chemicals were used for synthesis without further purification:  $\text{Sr}(\text{NO}_3)_2$  (Molar Chemicals, Halásztelek, Hungary; >99%), titanium isopropoxid ( $\text{C}_{12}\text{H}_{28}\text{O}_4\text{Ti}$ ) (Sigma Aldrich, St. Louis, MO, USA; >99%),  $\text{Cu}(\text{NO}_3)_2 \times 3 \text{H}_2\text{O}$  (Molar Chemicals, Halásztelek, Hungary; >99%),  $\text{Na}_2\text{WO}_4 \times 2 \text{H}_2\text{O}$  (Chinoin, Budapest; >99%), KOH (Molar Chemicals, Halásztelek, Hungary; >99%) and ultrapure Millipore Milli-Q water (Budapest, Hungary).  $\text{CuWO}_4$ -modified strontium titanate (CWSX) samples were prepared using a hydrothermal co-crystallization procedure, which is a relatively cheap and resizable method. The synthesis was performed by combining two recipes [16,29]. First modified sample, CWS0.5, was prepared as follows: First, we prepared solution A: 2.842 g  $\text{C}_{12}\text{H}_{28}\text{O}_4\text{Ti}$  dissolved in 50 mL 2-propanol. Solution B: 2.111 g  $\text{Sr}(\text{NO}_3)_2$  was dissolved in 50 mL  $\text{H}_2\text{O}$ . Dispersion C: 0.00922 g of  $\text{CuWO}_4$  dispersion was precipitated by adding the necessary copper and tungsten precursors ( $\text{Cu}(\text{NO}_3)_2 \times 3 \text{H}_2\text{O}$  and  $\text{Na}_2\text{WO}_4 \times 2 \text{H}_2\text{O}$ ) in stoichiometric amounts to 10 mL of water. Solution D: 50 mL 0.4 mol/L KOH solution. During the synthesis, dispersion C was added to solution B, and then the obtained dispersion E was added to solution A dropwise under vigorous stirring (dispersion F). Next, solution D was added to dispersion F. The mixture was kept at 90 °C for 1 h, and then it was loaded into a Teflon-lined autoclave which was kept at 200 °C for 3 h. After washing and drying the photocatalyst, the sample was calcined at 500 °C for 3 h in the presence of air. The product was 1.844 g of  $\text{SrTiO}_3$  with 0.5 wt%  $\text{CuWO}_4$ . In the case of the other samples, the preparation procedure was the same, with the only difference being that we systematically prepared more  $\text{CuWO}_4$  precipitates; the values are in Table 1. CWS0 was the reference; no  $\text{CuWO}_4$  precipitate was added during the synthesis. According to this procedure, we tried to carry out the synthesis with the minimum number of steps, and the energy requirement was mainly due to the double heat treatment.

### 3.2. Characterization

The  $\text{CuWO}_4\text{-SrTiO}_3$  sample crystallinity was determined with X-ray diffraction measurements, which were carried out with a Philips X-ray diffractometer (PW 1830 generator, PW 1820 goniometer,  $\text{CuK}\alpha$ :  $\lambda = 0.1542$  nm, 40–50 kV, 30–40 mA) (Philips, Germany), from 20 to  $80^\circ$  ( $2\theta$ ), at room temperature.

For optical characterization, the diffuse reflectance spectra were recorded with UV–VIS USB4000 type (Ocean Optics Inc., Dunedin, FL, USA), diode array spectrophotometer. The spectra were recorded from 200 to 850 nm wavelength. The band gap values were determined using the Kubelka–Munk method.

The room-temperature photoluminescence (PL) emission spectra of the samples were recorded at 300 nm excitation wavelength using a Horiba Jobin Yvon Fluoromax-4 type spectrofluorometer (Horiba, Kyoto, Japan).

Energy-dispersive X-ray spectra were measured with Hitachi S-4700 scanning electron microscope (Tokyo, Japan) with Röntec EDX detector (30 keV). We also performed the mapping measurements with this instrument.

The specific surface area values of the samples were measured by the BET method from  $\text{N}_2$  adsorption isotherms ( $77 \pm 0.5$  K) with Micromeritics Gemini 2375 Surface Area Analyzer (Micromeritics, Norcross, GA, USA).

The electrophoretic mobility of the samples was also determined using a HORIBA SZ-100 Nanoparticle Analyzer (Horiba, Kyoto, Japan); a disposable carbon-coated electrode cell was used. The zeta-potential values were determined using the Smoluchowski model, from the measured data. The measured dispersion concentration was 0.001  $w/v\%$ . In addition to the CWS samples, we also measured the pure  $\text{CuWO}_4$ . The zeta-potential values provide useful information about the aqueous-phase hydrodynamic stability as well [30].

### 3.3. Photocatalytic Activity Measurements

The photocatalytic activity of the CWSX samples was measured in 50 mL aqueous suspension. Phenol was the model pollutant, and the experiments were performed in an opened glass reactor, at room temperature. The used UV light source (local  $\lambda_{\text{max}} = 366$  nm (Figure S2) was fixed at 5 cm distance from the surface of continuously stirred (3000 rpm) suspensions. The photocatalyst concentration in the suspension was 0.1 wt%, while the initial phenol concentration was 10 mg/L. The suspensions were irradiated for 120 min during the tests. The concentration of phenol was followed with an Agilent 1290 Infinity II liquid chromatograph with UV detector (detection wavelength was 254 nm), the column was an InfinityLab Poroshell 120 ECsingle bondC18, while the mobile phase was 50/50 acetonitrile/water with 1 mL/min flow rate. Before the irradiation, the suspensions were kept in the dark for 30 min to ensure the adsorption equilibrium. Before chromatographic measurement, the collected samples were centrifuged two times (14,500 rpm, 5 min) and filtered through 0.1  $\mu\text{m}$  Millex-VV PVDF filter.

### 3.4. Detection of Hydroxyl Radical

The reaction between coumarin and hydroxyl radical produces 7-hydroxycoumarin (Figure 8) [28], which can be monitored spectrofluorometrically ( $\lambda_{\text{em, max}} = 453$  nm), and the amount of produced 7-hydroxycoumarin depends only on the hydroxyl radical concentration. The capacity of the hydroxyl radical production was measured on reference CWS0 and the best CWSX (the best photocatalyst in this work) sample, which was CWS2.5. The experiments were preceded by the calibration of spectrofluorometer with 7-hydroxycoumarin; the concentration dependence was linear over the range used ( $1 \times 10^{-8}$  mol/L– $5 \times 10^{-6}$  mol/L),  $R^2 = 0.9999$ .



**Author Contributions:** Á.Á.: Conceptualization, methodology, investigation, original draft. L.J.: Funding acquisition, writing—review and editing. All authors have read and agreed to the published version of the manuscript.

**Funding:** The authors are very thankful for the financial support from the National Research, Development and Innovation Office (GINOP-1.1.2-PIACI-KFI-2021-00193) and the Hungarian Scientific Research Fund (OTKA) FK 142437. This paper was also supported by the UNKP-22-5 New National Excellence Program of the Ministry for Innovation and Technology from the National Research, Development and Innovation Fund and by the János Bolyai Research Scholarship of the Hungarian Academy of Sciences. Áron Ágoston thanks for the support of the Hungarian NTP-NFTÖ-22-B-0025 scholarship.

**Data Availability Statement:** Not applicable.

**Conflicts of Interest:** The authors declare that they have no known competing financial interest or personal relationships that could have appeared to influence the work reported in this paper.

## References

1. Rodriguez, C.; Di Cara, A.; Renaud, F.N.R.; Freney, J.; Horvais, N.; Borel, R.; Puzenat, E.; Guillard, C. Antibacterial Effects of Photocatalytic Textiles for Footwear Application. *Catal. Today* **2014**, *230*, 41–46. [[CrossRef](#)]
2. Mills, A.; Davies, R.H.; Worsley, D. Water Purification by Semiconductor Photocatalysis. *Chem. Soc. Rev.* **1993**, *22*, 417–425. [[CrossRef](#)]
3. Ali, H.; Zaman, S.; Majeed, I.; Kanodarwala, F.K.; Nadeem, M.A.; Stride, J.A.; Nadeem, M.A. Porous Carbon/RGO Composite: An Ideal Support Material of Highly Efficient Palladium Electrocatalysts for the Formic Acid Oxidation Reaction. *ChemElectroChem* **2017**, *4*, 3126–3133. [[CrossRef](#)]
4. Zhou, Y.; Wang, Z.; Huang, L.; Zaman, S.; Lei, K.; Yue, T.; Li, Z.A.; You, B.; Xia, B.Y. Engineering 2D Photocatalysts toward Carbon Dioxide Reduction. *Adv. Energy Mater.* **2021**, *11*, 2003159. [[CrossRef](#)]
5. Noureen, L.; Xie, Z.; Gao, Y.; Li, M.; Hussain, M.; Wang, K.; Zhang, L.; Zhu, J. Multifunctional Ag<sub>3</sub>PO<sub>4</sub>-RGO-Coated Textiles for Clean Water Production by Solar-Driven Evaporation, Photocatalysis, and Disinfection. *ACS Appl. Mater. Interfaces* **2020**, *12*, 6343–6350. [[CrossRef](#)]
6. Sasikala, R.; Kandasamy, M.; Suresh, S.; Ragavendran, V.; Sasirekha, V.; Pearce, J.M.; Murugesan, S.; Mayandi, J. Enhanced Dye-Sensitized Solar Cell Performance Using Strontium Titanate Perovskite Integrated Photoanodes Modified with Plasmonic Silver Nanoparticles. *J. Alloys Compd.* **2021**, *889*, 161693. [[CrossRef](#)]
7. Ágoston, Á.; Balog, Á.; Narbutas, Š.; Dékány, I.; Janovák, L. Optimization of Plasmonic Copper Content at Copper-Modified Strontium Titanate (Cu-SrTiO<sub>3</sub>): Synthesis, Characterization, Photocatalytic Activity. *Catalysts* **2022**, *12*, 1041. [[CrossRef](#)]
8. Farré, M.J.; Franch, M.I.; Malato, S.; Ayllón, J.A.; Peral, J.; Doménech, X. Degradation of Some Biorecalcitrant Pesticides by Homogeneous and Heterogeneous Photocatalytic Ozonation. *Chemosphere* **2005**, *58*, 1127–1133. [[CrossRef](#)] [[PubMed](#)]
9. Reydellet, L.-H.; Roche, P.; Glatli, D.C.; Etienne, B.; Jin, Y. Quantum Partition Noise of Photon-Created Electron-Hole Pairs. *Phys. Rev. Lett.* **2003**, *90*, 176803. [[CrossRef](#)] [[PubMed](#)]
10. Vieira, Y.; Leichtweis, J.; Foletto, E.L.; Silvestri, S. Reactive Oxygen Species-Induced Heterogeneous Photocatalytic Degradation of Organic Pollutant Rhodamine B by Copper and Zinc Aluminate Spinels. *J. Chem. Technol. Biotechnol.* **2020**, *95*, 791–797. [[CrossRef](#)]
11. He, R.A.; Cao, S.W.; Yu, J.G. Recent Advances in Morphology Control and Surface Modification of Bi-Based Photocatalysts. *Wuli Huaxue Xuebao/Acta Phys.-Chim. Sin.* **2016**, *32*, 2841–2870. [[CrossRef](#)]
12. Cravanzola, S.; Cesano, F.; Gaziano, F.; Scarano, D. Sulfur-Doped TiO<sub>2</sub>: Structure and Surface Properties. *Catalysts* **2017**, *7*, 214. [[CrossRef](#)]
13. Sakthivel, S.; Shankar, M.V.; Palanichamy, M.; Arabindoo, B.; Bahnemann, D.W.; Murugesan, V. Enhancement of Photocatalytic Activity by Metal Deposition: Characterisation and Photonic Efficiency of Pt, Au and Pd Deposited on TiO<sub>2</sub> Catalyst. *Water Res.* **2004**, *38*, 3001–3008. [[CrossRef](#)] [[PubMed](#)]
14. Syafiuddin, A.; Hadibarata, T.; Zon, N.F. Salmiati Characterization of Titanium Dioxide Doped with Nitrogen and Sulfur and Its Photocatalytic Appraisal for Degradation of Phenol and Methylene Blue. *J. Chin. Chem. Soc.* **2017**, *64*, 1333–1339. [[CrossRef](#)]
15. Rosy, A.; Kalpana, G. Reduced Graphene Oxide/Strontium Titanate Heterostructured Nanocomposite as Sunlight Driven Photocatalyst for Degradation of Organic Dye Pollutants. *Curr. Appl. Phys.* **2018**, *18*, 1026–1033. [[CrossRef](#)]
16. Xu, J.; Wei, Y.; Huang, Y.; Wang, J.; Zheng, X.; Sun, Z.; Fan, L.; Wu, J. Solvothermal Synthesis Nitrogen Doped SrTiO<sub>3</sub> with High Visible Light Photocatalytic Activity. *Ceram. Int.* **2014**, *40*, 10583–10591. [[CrossRef](#)]
17. Choi, Y.; Jung, M.; Lee, Y.K. Effect of Heating Rate on the Activation Energy for Crystallization of Amorphous Ge<sub>2</sub>Sb<sub>2</sub>Te<sub>5</sub> Thin Film. *Electrochem. Solid-State Lett.* **2009**, *12*, F17. [[CrossRef](#)]
18. Da Silva, L.F.; Avansi, W.; Moreira, M.L.; Mesquita, A.; Maia, L.J.Q.; Andrés, J.; Longo, E.; Mastelaro, V.R. Relationship between Crystal Shape, Photoluminescence, and Local Structure in SrTiO<sub>3</sub> Synthesized by Microwave-Assisted Hydrothermal Method. *J. Nanomater.* **2012**, *2012*, 890397. [[CrossRef](#)]

19. WEITZEL, H. Kristallstrukturverfeinerung von Wolframiten Und Columbiten. *Zeitschrift für Krist.-Cryst. Mater.* **1976**, *144*, 238–258. [[CrossRef](#)]
20. Gillespie, J.B.; Lindberg, J.D.; Laude, L.S. Kubelka-Munk Optical Coefficients for a Barium Sulfate White Reflectance Standard. *Appl. Opt.* **1975**, *14*, 807–809. [[CrossRef](#)]
21. Lévy, F.; Mercier, A.; Voitchovsky, J.P. Band-Edge Photoluminescence of PbI<sub>2</sub>. *Solid State Commun.* **1974**, *15*, 819–822. [[CrossRef](#)]
22. Siebenhofer, M.; Viernstein, A.; Morgenbesser, M.; Fleig, J.; Kubicek, M. Photoinduced Electronic and Ionic Effects in Strontium Titanate. *Mater. Adv.* **2021**, *2*, 7583–7619. [[CrossRef](#)] [[PubMed](#)]
23. Wu, Z.; Zhao, Z.; Cheung, G.; Doughty, R.M.; Ballestas-Barrientos, A.R.; Hirmez, B.; Han, R.; Maschmeyer, T.; Osterloh, F.E. Role of Surface States in Photocatalytic Oxygen Evolution with CuWO<sub>4</sub> Particles. *J. Electrochem. Soc.* **2019**, *166*, H3014–H3019. [[CrossRef](#)]
24. Balassa, L.; Ágoston, Á.; Kása, Z.; Hornok, V.; Janovák, L. Surface Sulfate Modified TiO<sub>2</sub> Visible Light Active Photocatalyst for Complex Wastewater Purification: Preparation, Characterization and Photocatalytic Activity. *J. Mol. Struct.* **2022**, *1260*, 132860. [[CrossRef](#)]
25. Shukla, S.; Pandey, H.; Singh, P.; Tiwari, A.K.; Baranwal, V.; Pandey, A.C. Synergistic Impact of Photocatalyst and Dopants on Pharmaceutical-Polluted Waste Water Treatment: A Review. *Environ. Pollut. Bioavailab.* **2021**, *33*, 347–364. [[CrossRef](#)]
26. Zhang, M.; Yu, H.; Lyu, M.; Wang, Q.; Yun, J.-H.; Wang, L. Composition-Dependent Photoluminescence Intensity and Prolonged Recombination Lifetime of Perovskite CH<sub>3</sub>NH<sub>3</sub>PbBr<sub>3-x</sub>Cl<sub>x</sub> Films. *Chem. Commun* **2014**, *50*, 11727. [[CrossRef](#)]
27. Jayathilaka, P.B.; Pathiraja, G.C.; Bandara, A.; Subasinghe, N.D.; Nanayakkara, N. Theoretical Study of Phenol and Hydroxyl Radical Reaction Mechanism in Aqueous Medium by the DFT/B3LYP/6-31+G(d,p)/CPCM Model. *Can. J. Chem.* **2014**, *92*, 809–813. [[CrossRef](#)]
28. Maier, A.C.; Iglebaek, E.H.; Jonsson, M. Confirming the Formation of Hydroxyl Radicals in the Catalytic Decomposition of H<sub>2</sub>O<sub>2</sub> on Metal Oxides Using Coumarin as a Probe. *ChemCatChem* **2019**, *11*, 5435–5438. [[CrossRef](#)]
29. Pourmortazavi, S.M.; Rahimi-Nasrabadi, M.; Khalilian-Shalamzari, M.; Ghaeni, H.R.; Hajimirsadeghi, S.S. Facile Chemical Synthesis and Characterization of Copper Tungstate Nanoparticles. *J. Inorg. Organomet. Polym. Mater.* **2014**, *24*, 333–339. [[CrossRef](#)]
30. Gallardo, V.; Morales, M.E.; Ruiz, M.A.; Delgado, A.V. An Experimental Investigation of the Stability of Ethylcellulose Latex: Correlation between Zeta Potential and Sedimentation. *Eur. J. Pharm. Sci.* **2005**, *26*, 170–175. [[CrossRef](#)]

**Disclaimer/Publisher's Note:** The statements, opinions and data contained in all publications are solely those of the individual author(s) and contributor(s) and not of MDPI and/or the editor(s). MDPI and/or the editor(s) disclaim responsibility for any injury to people or property resulting from any ideas, methods, instructions or products referred to in the content.